
DRAFT

CMS Physics Analysis Summary

The content of this note is intended for CMS internal use and distribution only

October 11, 2008

Archive Id:

Archive Date:

Transverse Momentum Distribution within Jets in pp collisions at 14 TeV

The CMS collaboration

Abstract

The CMS (Compact Muon Solenoid) detector will observe high transverse momentum jets produced in the final state of proton-proton collisions at the center of mass energy of 14 TeV. These data will allow us to measure jet shapes, defined as the fractional transverse momentum distribution as a function of the distance from the jet axis. Since jet shapes are sensitive to parton showering processes they provide a good test of Monte Carlo event simulation programs. In this note we present a study of jet shapes reconstructed using calorimeter energies where the statistics of all distributions correspond to a CMS data set with 10 pb^{-1} of integrated luminosity. We compare the predictions of the Monte Carlo generators PYTHIA and HERWIG++.

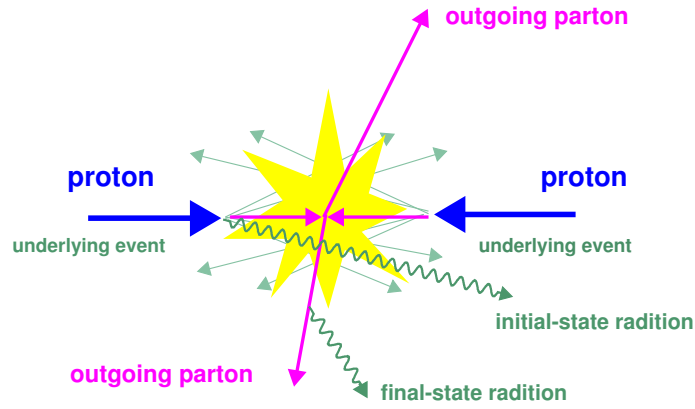


Figure 1: Illustration of a typical proton-proton two parton hard scattering event. including initial and final state radiation and beam-beam remnants. The underlying event is defined as everything except the two outgoing hard scattered jets.

1 Introduction

The transverse momentum profile of a jet, or jet shape [1, 2], is sensitive to multiple parton emissions from the primary outgoing parton and provides a good test of the parton showering description of Quantum Chromodynamics (QCD), the theory of strong interactions. Historically the jet shape has been used to test perturbative QCD (pQCD) α_s^3 calculations [3, 4]. These leading order calculations, with only one additionally gluon in a jet, showed good agreement with the observed jet shapes.

While confirming the validity of pQCD calculations, jet shape studies also indicated that jet clustering, underlying event contribution and hadronization effects must be considered. These effects can be modeled accurately within the framework of full-event generators. Current Monte Carlo (MC) event generators use pQCD inspired parton shower models, in conjunction with hadronization and underlying event models, to generate final state particles. MC generators are used extensively to model signal and background events in most analyses at hadron colliders. Jet shapes can be used to tune phenomenological parameters in these MC generators.

QCD predicts broader gluon jets than quark jets because the strength of the the gluon-gluon coupling is larger than that of the quark-gluon coupling. The structure of quark and gluon jets can be investigated by comparing measurements of the jet shapes in different processes enriched with either quark or gluon initiated jets in the final state. Previously, jet shapes have been measured in $p\bar{p}$ collisions at Tevatron and ep collisions at HERA [5–7].

In this paper, we present a study of jet shapes at particle and calorimeter levels in the central region of the CMS detector and compare the results obtained with various MC generators. The sensitivities of jet shapes to the underlying event (UE) model and to the flavour of the initiating parton are also explored.

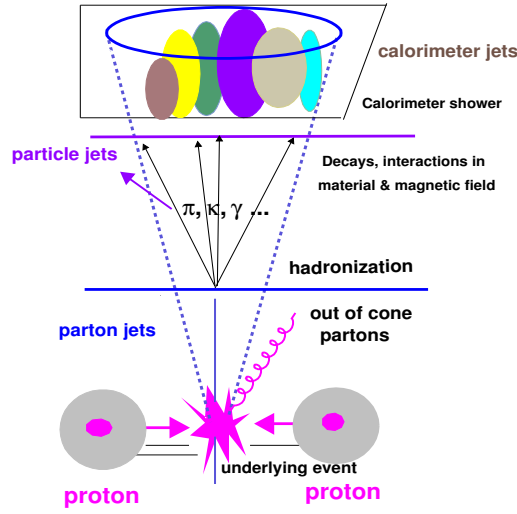


Figure 2: Schematic of jet evolution and detection. Parton jets hadronize into particle jets which interact in the calorimeter forming calorimeter jets.

2 Jet Clustering Algorithm and Data Samples

In high energy collisions partons are produced in the final state with large transverse momenta as a result of the hard scattering process illustrated in Fig. 1. Partons outgoing from the interaction point produce parton showers and subsequently partons from these showers combine to form hadrons which interact in the detector (see Fig. 2.) QCD dijet events were generated with PYTHIA [8] ($15 < \hat{p}_T < 5000$ GeV), ALPGEN [9] ($20 < \hat{p}_T < 5600$ GeV) and HERWIG++ [10] ($50 < \hat{p}_T < 7000$ GeV). Results of this study extend up to jet $P_T = 1.4$ TeV which is the approximate sensitivity limit for a 10 pb^{-1} integrated luminosity sample of LHC collisions at 14 TeV.

The quark and gluon jet fractions as predicted by PYTHIA as a function of the jet P_T are plotted in Fig. 3.

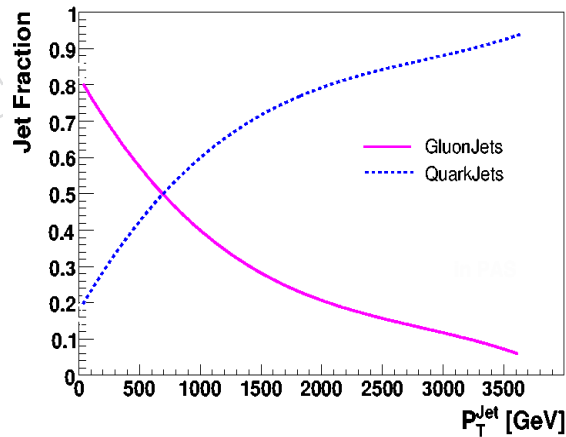


Figure 3: Fraction of quark or gluon initiated jets as a function of jet P_T (from PYTHIA).

36 In this analysis, jets are defined as amount of energy deposited in the cone of radius $R =$
 37 $\sqrt{(\Delta y)^2 + (\Delta\phi)^2}$ in (y, ϕ) space, where Δy and $\Delta\phi$ specify the cone dimensions in rapidity [11]
 38 and azimuth respectively. For this study, $R=0.7$ is used.

39 The jet kinematics are determined by reconstructing the jet at particle or calorimeter level us-
 40 ing the SISCone algorithm [12]. In contrast to traditional clustering algorithms which develop
 41 stable cones iteratively starting with particles above a certain threshold (seeds), the SISCone al-
 42 gorithm searches for all stable cones. We use calorimeter energy deposits to explore the largest
 43 P_T range possible. Tracks cones can be used to measure jet shapes at low and medium P_T ,
 44 and to help estimate systematic uncertainties. The calorimeter jet P_T is corrected using CMS
 45 standard jet energy correction [13]. Calorimeter towers and reconstructed tracks are required to
 46 satisfy the $E_T=0.5$ GeV threshold while no threshold is applied to particles when reconstructing
 47 generator-level jets.

48 3 Jet Shapes

49 The jet shape is defined as the average fraction of the jet transverse momentum within a cone
 50 of a given size r around the jet axis, $r = \sqrt{(y_i - y_j)^2 + (\phi_i - \phi_j)^2}$, where i refers to the particle,
 51 calorimeter tower or track, and j to the jet axis. Jet shapes can be studied by using an integrated
 52 or a differential distribution. Here we present results for the integrated jet shapes. Only events
 53 are considered for which the two highest P_T (leading) jets are within $|y| < 1$. All particles and
 54 calorimeter towers within a distance of $R=0.7$ from the jet axis are used. This large cone size
 55 ensures that most of the parent parton energy is included in the jet.

56 The integrated jet shapes (see Fig. 4), ψ^{CAL} and $\psi^{PARTICLE}$ corresponding to calorimeter tower
 57 and particle energies respectively, are defined as:

$$\psi(r) = \frac{1}{N_{jets}} \sum_{jets} \frac{P_T(0,r)}{P_T(0,R)} \quad (1)$$

58 where $P_T(0,r)$ is the scalar sum of transverse momenta of all particles within the distance r
 59 from the jet axis with $\psi(R=r) = 1$.

60 Due to various detector effects, measured (calorimeter) jet shapes are different than the true
 61 (particle) jet shapes. Due to the magnetic field of CMS, charged particles with $P_T < 0.9$ GeV
 62 do not reach the calorimeter. In addition showers from a particle interacting with detector
 63 material will spread their energy over many calorimeter towers. The measured jet shapes must
 64 be corrected for these detector effects. Correction factors were determined as a function of
 65 distance from the jet axis using MC events before and after the CMS detector simulation. For
 66 this approach to be valid, the MC simulation must describe the calorimeter response accurately.
 67 In section 4 we discuss a method to cross check the accuracy of calorimeter simulation using
 68 tracking information.

69 Fig. 5 shows the corrected integrated jet shapes in selected P_T bins. Corrected jet shapes agree
 70 very well with particle jets by construction. The jet shape $\psi(r)$ increases faster with r for jets at
 71 larger P_T indicating that larger P_T jets are more collimated.

72 We tested the correction derived from PYTHIA on an independent sample generated using
 73 ALPGEN [9]. In this sample the parton showering and hadronization models are the same as
 74 used by PYTHIA. Fig. 6 shows the corrected integrated jet shapes at particle and calorimeter
 75 level for ALPGEN multijet samples. The correction factors determined from PYTHIA events

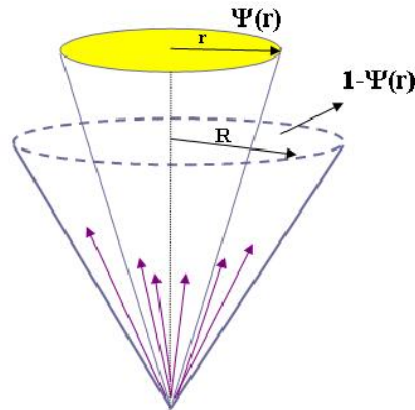


Figure 4: Definition of the integrated jet shape, $\psi(r)$.

76 work reasonably well for ALPGEN, as expected since the parton showering and hadronization
77 is done by PYTHIA.

78 Jet shapes are sensitive to quark and gluon jet contributions. Using parton information from
79 PYTHIA we classify hadron level jets based on matching within $\Delta R < 0.5$ in (y, ϕ) space. The
80 MC predicts that the measured jet shapes are dominated by contributions from gluon initiated
81 jets at low jet P_T while contributions from quark initiated jets become important at high jet
82 P_T . Fig. 7 compares the integrated jet shapes for quarks and gluons with simulated data. As
83 expected, quark jets are narrower than the gluon jets due to the coupling strengths for gluon
84 emission which depend on the color factors $C_F=4/3$ for radiating quarks and $C_A=3$ for gluons.

85 It is therefore expected that jets produced by quarks or gluons will also show differences in
86 their average multiplicity and in the shape of their hadronic momentum spectra.

87 Fig. 9 presents the P_T fraction contained in the jet cone of $R = 0.7$ lying outside a cone of
88 $r=0.2$ as function of the jet P_T . Reconstructed calorimeter jets from the full CMS Monte Carlo
89 simulation are compared with parton shower MC predictions for quark and gluon jets.

90 3.1 Sensitivity of Jet Shapes to different Underlying Event Tunes

91 The energy from the underlying event (UE) contributes to jets and impacts the jet shapes. To
92 determine the sensitivity of jet shapes to the UE contribution, event samples were generated
93 using PYTHIA DW which has a less active UE contribution than PYTHIA with tune DWT,
94 which is the CMS default setting [14]. These tunes use different extrapolations to $\sqrt{s}=14$ TeV
95 from the same tune at the Tevatron energy $\sqrt{s}=1.8$ TeV. The jet shapes for PYTHIA DWT and
96 PYTHIA DW are shown in Fig. 8. One can observe the difference in jet shapes due to the UE
97 contribution at low jet P_T only.

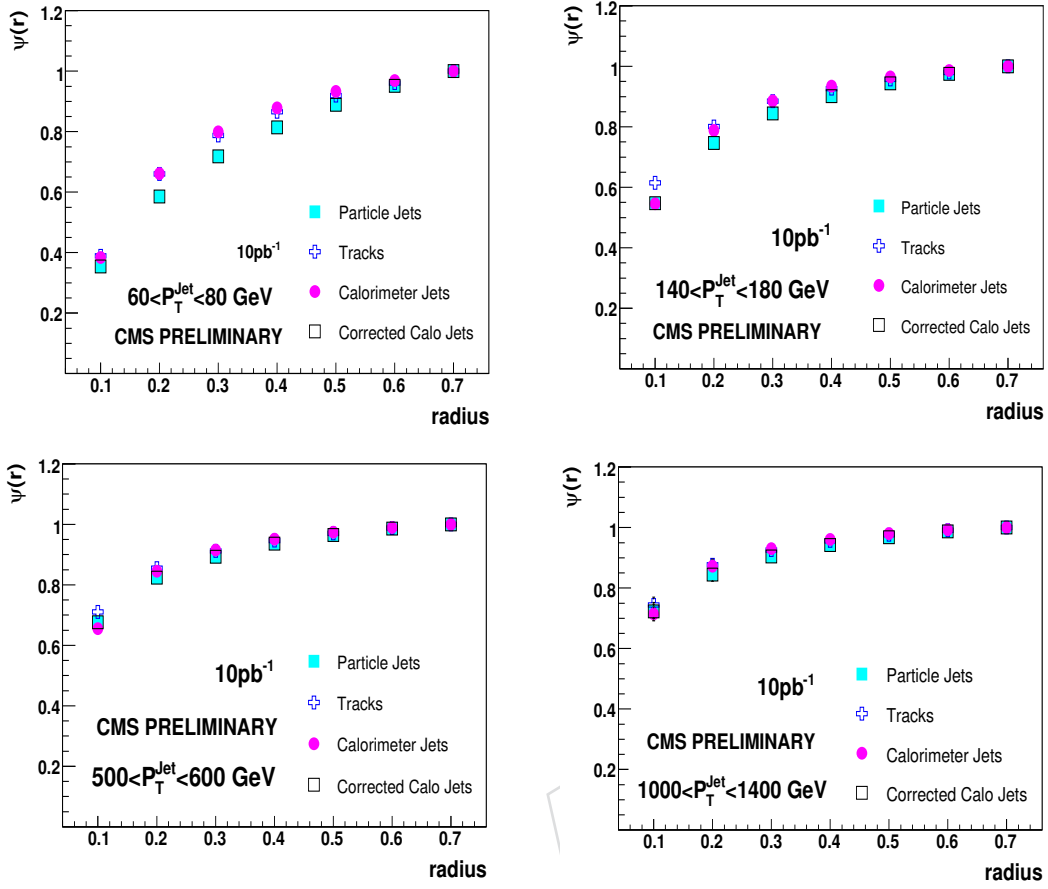


Figure 5: Integrated jet shapes for selected P_T^{jet} bins. Statistical errors are included.

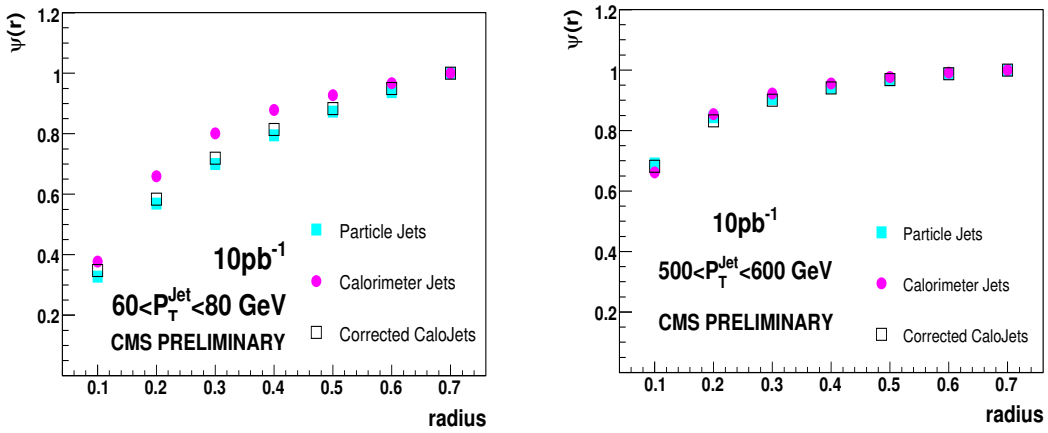


Figure 6: Integrated jet shapes for different P_T^{jet} bins in multijet samples generated with ALPGEN. Calorimeter jets are corrected using corrections derived from PYTHIA samples. Statistical errors are included.

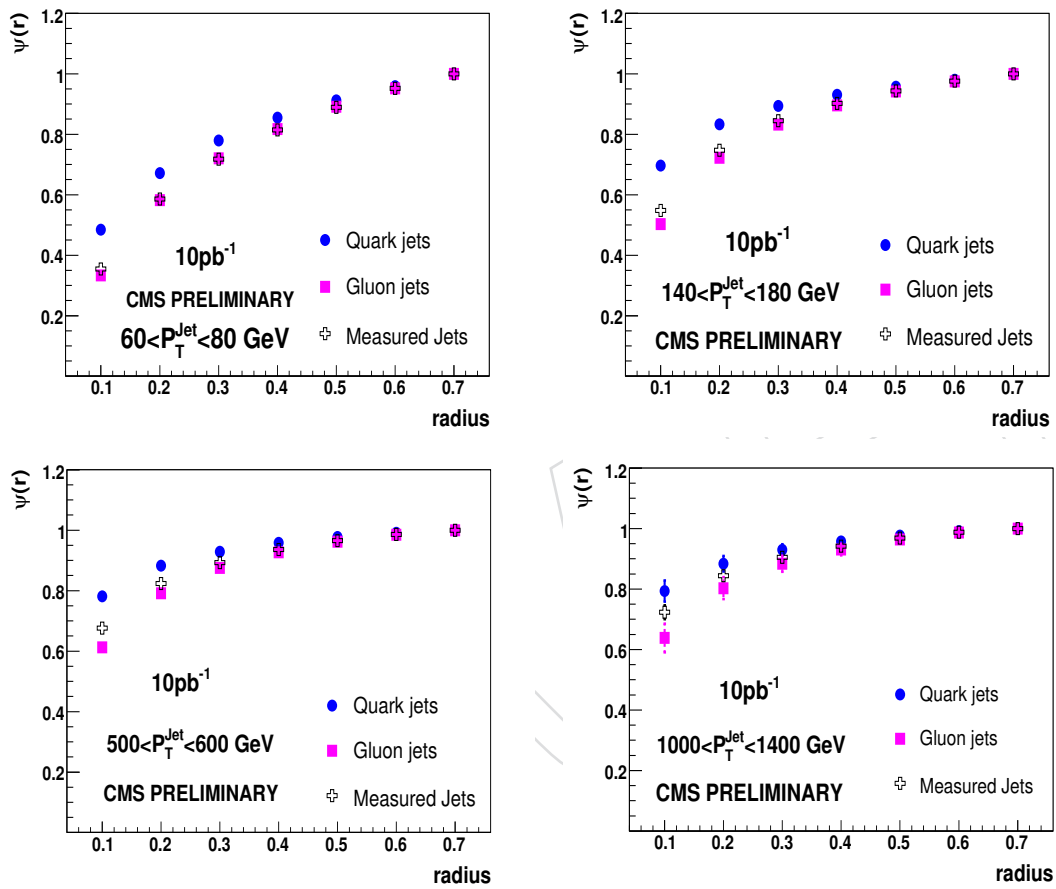


Figure 7: Comparison of quark and gluon integrated jet shapes to simulated data in selected P_T^{jet} bins. Statistical errors are included.

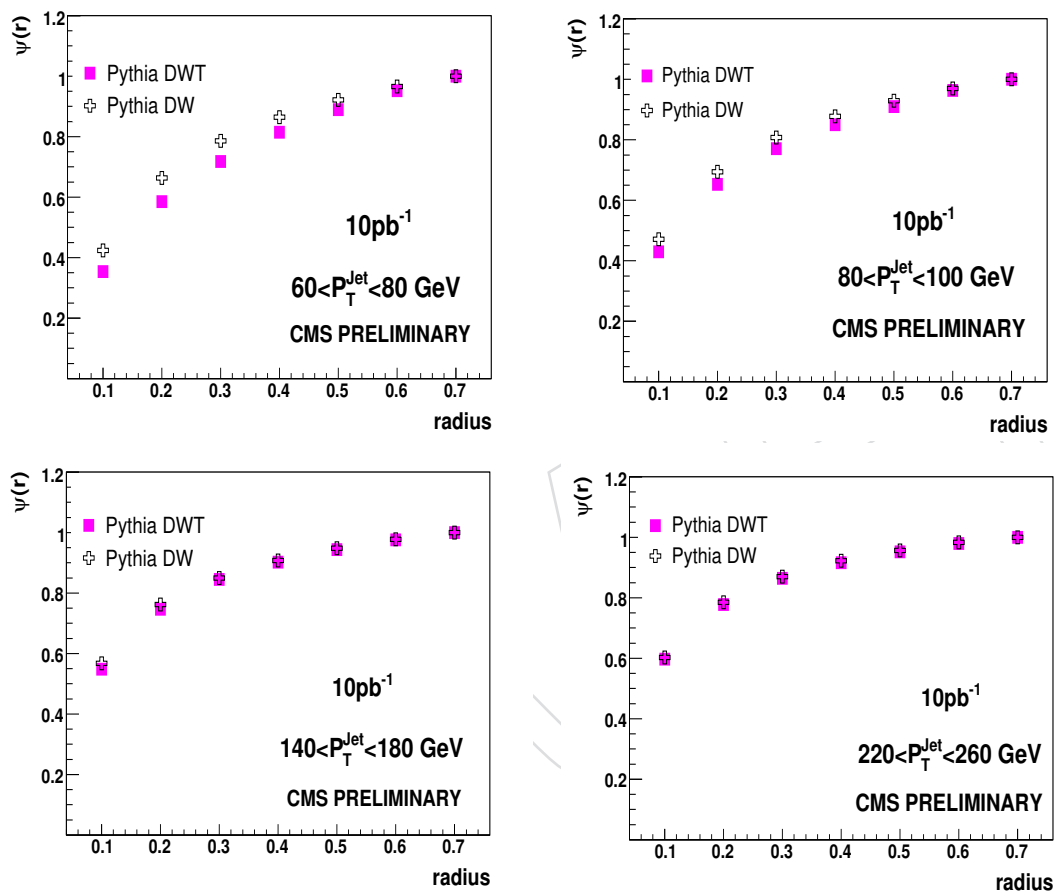


Figure 8: Comparison of jet shapes for PYTHIA tunes DW and DWT at particle level in selected P_T^{jet} bins. Statistical errors are included.

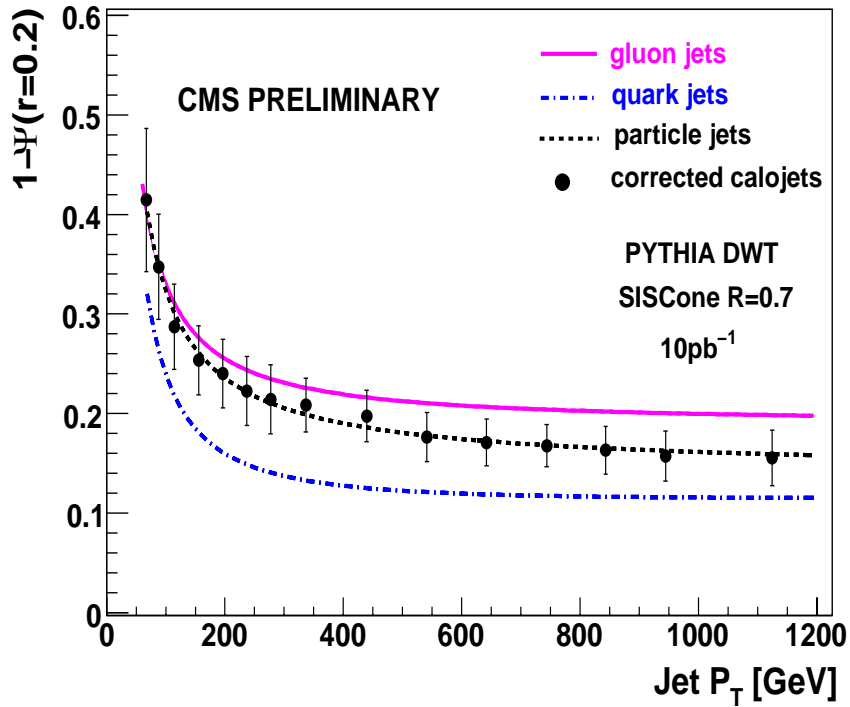


Figure 9: The fractional transverse momentum of a jet outside $r=0.2$, $1-\psi(0.2)$, as a function of the jet P_T for jets in the rapidity region $|y| < 1$. The reconstructed calorimeter jets, from PYTHIA Tune DWT (black points) are shown along with PYTHIA predictions for quark fraction (dashed-dotted line) gluon fraction (solid line) and total (solid) initiated jets. The statistical uncertainty on each point is calculated as rms/\sqrt{N} where rms is calculated from the distribution of $\psi(0.2)$ in each P_T bin and N is the number of expected jets in the bin for a luminosity of 10 pb^{-1} . Systematic and statistical errors for the reconstructed calorimeter jets are added in quadrature. For the integrated shape the uncertainties at different r points are partially correlated.

4 Systematic Uncertainties

The main sources of systematic uncertainty on the jet shape measurement are: calorimeter response to particles, overall jet energy scale (JES) and jet fragmentation model. The uncertainties arising from the jet position resolution and jet/event selection cuts are expected to be negligible compared to the sources listed above and are not considered.

4.1 Jet Energy Scale

The uncertainty on the jet energy scale will be determined from the data [8]. Current expectation of the JES uncertainty at start up is $\pm 10\%$. Changing the JES correction by $\pm 10\%$ changes the jet shapes as jets migrate between different P_T bins. The uncertainty on the jet shape is 10% at $r=0.1$, 5% at $r=0.2$ for $P_T < 100$ GeV, and decreases as a function of r while it is $< 2\%$ at $r=0.1$ for $P_T > 100$ GeV and negligible at $r > 0.1$. (The systematic uncertainty at $r=0.7$ is 0 by definition).

4.2 Jet Fragmentation

Because the calorimeter response depends on the energies of the particles in the jets, modeling of jet fragmentation contributes to the uncertainty. Particle level jet shapes in PYTHIA DWT and HERWIG++ 2.2 [15] are shown in Fig. 10. Their observed difference is less than 5% at $r < 0.3$ and decreases as a function of r . The model of the underlying event used in HERWIG++ is described in [10, 16].

To determine the associated systematic uncertainty, we compared the event shape correction factors for the PYTHIA DWT and HERWIG++ samples. We found them to agree within 5% (2%) at $r=0.1$ (0.2) for $60 < P_T < 80$ GeV. For $P_T > 80$ GeV the differences range between 5 – 10% at $r=0.1$ and $< 5\%$ at $r=0.2$. These differences decrease with increasing radius r for the all jet P_T .

4.3 Non-linearity of Calorimeter Response and Transverse Shower Profile

The uncertainties due to CMS calorimeter simulation can be estimated by comparing track jet shapes with calorimeter jet shapes in simulated and collider data. Here we assume that track reconstruction inefficiency and fake rates are small in both data and MC and have negligible effect on track jet shapes. These assumptions will be verified by comparing the track multiplicity and track P_T distributions in data and MC after applying the track reconstruction inefficiency and fake rate as measured from data. We will measure the same ratio in data and determine the scale factor SF as defined below. This scale factor quantifies the difference between the data and the simulation and if it is ~ 1 , we plan to scale the MC derived corrections by SF and add the deviation from unity as a systematic uncertainty.

$$R^{MC} = \frac{TrackJetShape}{CaloJetShape}_{MC}, \quad R^{DATA} = \frac{TrackJetShape}{CaloJetShape}_{DATA} \quad (2)$$

$$SF = \frac{R^{DATA}}{R^{MC}} \quad (3)$$

In the absence of data, we have estimated the size of this uncertainty using a simple model. We determined the jet shapes by propagating particles to the calorimeter and using a parameterized response. By varying the calorimeter average response to single particles $E^{CAL}/P_{particle}$ within reasonable limits, the calorimeter jet shape changes by $< 2\%$. The difference between

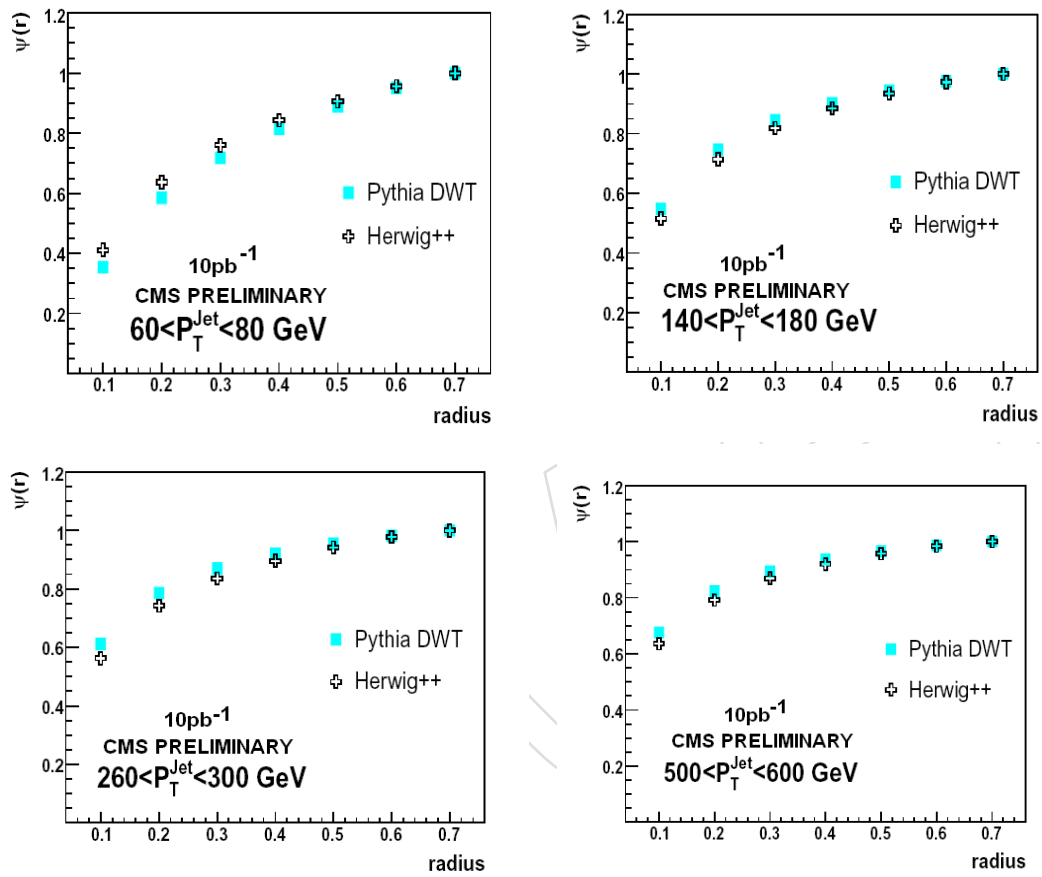


Figure 10: Comparison of integrated jet shapes from HERWIG++ and PYTHIA at particle level for selected P_T^{Jet} bins. Statistical errors are included.

135 jet shapes obtained using the full simulation and those obtained using the parameterized cal-
136 orimeter response (ignoring transverse shower spreading) is negligible for $r > 0.3$ for all jet P_T .
137 For $60 < P_T < 80$ GeV, the difference is 30% (10%) at $r=0.1$ (0.2) and decreases to 20% (10%) for
138 $r=0.1$ (0.2) for $80 < P_T < 100$ GeV jets. For jets with $P_T > 100$ GeV, the difference is 10% at $r=0.1$
139 and negligible for $r > 0.1$. In Fig. 9, these differences are added in quadrature with the other
140 sources of systematic uncertainty.

DRAFT

5 Conclusions

141

142 Using PYHTIA and HERWIG++ MC simulations, we have investigated a technique to measure
143 jet shapes in pp collisions for the two leading jets in the kinematic region $60 \text{ GeV} < P_T^{jet} < 1.4$
144 TeV and $|y| < 1$. Particle level jet shapes were determined from calorimeter jets using cor-
145 rections derived from PYTHIA MC events. Several sources of systematic uncertainties were
146 investigated, arising from jet energy calibration, jet fragmentation, calorimeter response and
147 transverse showering, as function of jet P_T and distance from jet axis r . The systematic uncer-
148 tainty is dominated by overall jet energy scale, jet fragmentation and calorimeter simulation.
149 The total systematic uncertainty at $r=0.2$ is 12% at $P_T=60$ GeV, decreasing to 4% at jet $P_T=1$ TeV.
150 Different underlying event tunes (PYTHIA DWT and PYTHIA DW) were studied. Both tunes
151 predict more quark jets and hence narrower jets at increasing jet P_T , however PYTHIA DW
152 tends to produce narrower jet shapes in the low P_T region. A measurement of the jet shapes in
153 the context of the PYTHIA Monte Carlo gives an estimate of the fraction of gluon initiated jets
154 in data as a function of jet P_T .

DRAFT

References

- 155
- 156 [1] S. D. Ellis, Z. Kunszt, and D. E. Soper, "Jets at hadron colliders at order α_s^3 : A
157 Look inside," *Phys. Rev. Lett.* **69** (1992) 3615–3618, arXiv:hep-ph/9208249.
158 doi:10.1103/PhysRevLett.69.3615.
- 159 [2] M. H. Seymour, "Jet shapes in hadron collisions: Higher orders, resummation and
160 hadronization," *Nucl. Phys.* **B513** (1998) 269–300, arXiv:hep-ph/9707338.
161 doi:10.1016/S0550-3213(97)00711-6.
- 162 [3] CDF Collaboration, F. Abe et al., "A Measurement of jet shapes in $p\bar{p}$ collisions at
163 $\sqrt{s} = 1.8$ TeV," *Phys. Rev. Lett.* **70** (1993) 713–717.
164 doi:10.1103/PhysRevLett.70.713.
- 165 [4] D0 Collaboration, S. Abachi et al., "Transverse energy distributions within jets in $p\bar{p}$
166 collisions at $\sqrt{s} = 1.8$ TeV," *Phys. Lett.* **B357** (1995) 500–508.
167 doi:10.1016/0370-2693(95)00889-S.
- 168 [5] CDF Collaboration, D. E. Acosta et al., "Study of jet shapes in inclusive jet production in
169 $p\bar{p}$ collisions at $\sqrt{s} = 1.96$ TeV," *Phys. Rev.* **D71** (2005) 112002,
170 arXiv:hep-ex/0505013. doi:10.1103/PhysRevD.71.112002.
- 171 [6] H1 Collaboration, C. Adloff et al., "Measurements of transverse energy flow in deep
172 inelastic scattering at HERA," *Eur. Phys. J.* **C12** (2000) 595–607,
173 arXiv:hep-ex/9907027. doi:10.1007/s100520000287.
- 174 [7] ZEUS Collaboration, J. Breitweg et al., "Measurement of jet shapes in high- Q^2 deep
175 inelastic scattering at HERA," *Eur. Phys. J.* **C8** (1999) 367–380, arXiv:hep-ex/9804001.
176 doi:10.1007/s100520050471.
- 177 [8] T. Sjostrand, S. Mrenna, and P. Skands, "PYTHIA 6.4 physics and manual," *JHEP* **05**
178 (2006) 026, arXiv:hep-ph/0603175.
- 179 [9] M. L. Mangano, M. Moretti, F. Piccinini, R. Pittau, and A. D. Polosa, "ALPGEN, a
180 generator for hard multiparton processes in hadronic collisions," *JHEP* **07** (2003) 001,
181 arXiv:hep-ph/0206293.
- 182 [10] M. Bahr, S. Gieseke, and M. H. Seymour, "Underlying events in Herwig++,"
183 arXiv:0809.2669.
- 184 [11] The coordinate system used at CMS is defined as follows: the x -axis points horizontally
185 outside the LHC ring, the y -axis points upwards, and the z -axis is aligned with the
186 nominal beam direction. The azimuthal angle is ϕ and the polar angle is θ . The transverse
187 momentum P_T is defined as a projection of a particle momentum P on the xy -plane,
188 $P_T = P \cdot \sin \theta$. The rapidity is defined as $y = \frac{1}{2} \log \frac{E+P_z}{E-P_z}$, where E denotes the energy and
189 P_z is the component of the momentum along the z direction.
- 190 [12] G. P. Salam and G. Soyez, "A practical Seedless Infrared-Safe Cone jet algorithm," *JHEP*
191 **05** (2007) 086, arXiv:0704.0292.
- 192 [13] CMS Collaboration, "Plans for Jet Energy Corrections at CMS,". CMS-PAS-JME-007-002.
- 193 [14] CMS Collaboration, "The Underlying Event at LHC,". CMS-Note-2006/067.
- 194 [15] M. Bahr et al., "Herwig++ 2.2 Release Note," arXiv:0804.3053.

- 195 [16] M. Bahr, S. Gieseke, and M. H. Seymour, "Simulation of multiple partonic interactions in
196 Herwig++," *JHEP* **07** (2008) 076, arXiv:0803.3633.
197 doi:10.1088/1126-6708/2008/07/076.

DRAFT